PANS SIMULATIONS: LOW VERSUS HIGH REYNOLDS NUMBER APPROACH

MAARTEN KLAPWIJK*†‡, THOMAS LLOYD‡, GUILHERME VAZ‡ and TOM van TERWISGA†‡

† Faculty of Mechanical, Maritime and Material Engineering
Delft University of Technology
Mekelweg 5, 2628 CD Delft, The Netherlands
e-mail: m.d.klapwijk@tudelft.nl, web page: http://www.tudelft.nl/

‡ Maritime Research Institute Netherlands (MARIN)
Haagsteeg 2, 6708 PM Wageningen, The Netherlands
e-mail: m.klapwijk@academy.marin.nl, web page: http://www.marin.nl/

Key words: PANS, Turbulent channel flow, ReFRESCO, CFD

Abstract. Different approaches for specifying the ratio of modelled-to-total dissipation (f_ε) in the PANS model, based on the $k-\omega$ SST model, are evaluated for different ratios of the modelled-to-total kinetic energy, f_k. Based on theoretical reasoning it is argued that applying $f_\varepsilon = a \cdot f_k$ should have little effect, and that $f_\varepsilon = f_k$ is not expected to improve the results. This is confirmed by applying the approaches to a turbulent channel flow at $Re_\tau = 395$ and 180, and comparing the results to the often used 'high Reynolds number' approach ($f_\varepsilon = 1.0$). Reducing f_ε leads to a reduction in range of scales in the flow; dissipation is allowed at larger scales and therefore smaller scales are suppressed.

1 INTRODUCTION

The application of high fidelity turbulence models for industrial problems, such as cavitation calculations, is mostly focused on the use of *hybrid* models such as Detached Eddy Simulation (DES) based models. These models switch between Reynolds Averaged Navier-Stokes (RANS) and Large Eddy Simulation (LES) based on the local grid size, wall distance and RANS length scale, with the aim of improving the accuracy compared to full RANS. However this approach may lead to commutation errors in the transition between the two zones, and is highly grid dependent due to the zonal formulation. In addition numerical error quantification is made difficult due to entanglement of the modelling and discretisation errors. *Bridging* models, such as Partially Averaged Navier-Stokes (PANS), are an alternative approach without these problems. The PANS model can operate at any degree of physical resolution, independent of the grid, by setting the modelled-to-total ratios of turbulence kinetic energy (f_k) and dissipation (f_ε) [1]. In literature, the model is applied almost exclusively using $f_k \ll 1$ and $f_\varepsilon = 1.0$ (known as the 'high Reynolds number' approach), an exception being the work of [2] and [3]. This approach assumes that the PANS cut-off is located at lower wave numbers than the dissipation range and therefore that the dissipation occurs entirely at the modelled scales. This is valid if there is a clear separation between the large energy containing scales and the small dissipative scales (identifiable by the inertial subrange, which fol-

lows Kolmogorov's law) [1, 3]. Theoretically, for low Reynolds number flows, where the scales overlap, or for high Reynolds number flows with a high physical resolution (low f_k), part of the dissipation should also be resolved. This implies that f_ε should be lower than 1.0. It is expected that the resolved structures, obtained when $f_k < 1.0$, should change due to increased dissipation.

Although most maritime applications are high Reynolds number flows, it is not unlikely that some cases require high physical resolutions, i.e. low f_k. For low Reynolds numbers, an often mentioned approach is to keep $f_k = f_\varepsilon$, whereas for moderate Reynolds numbers, $f_k < f_\varepsilon < 1.0$ has been recommended [3, 4]. Pereira et al. [5] state that if $f_k = f_\varepsilon$ the only change with respect to the underlying RANS model is an increase of the effective diffusion coefficient and cross-diffusion term; these terms go infinity when f_k goes to 0. Using this approach vortex shedding for a cylinder was underpredicted, especially with lower f_k. By contrast Lakshmipathy et al. [3] obtained satisfactory results for the same test case using a finer grid, indicating a potential grid dependency. Frendi et al. [2] simulated a backward facing step, using a fixed f_k and varying f_ε. These authors state that for wall-bounded flows viscous effects and dissipation should be taken into account by lowering f_ε. Better agreement with experiments was reported with this approach, although only the parameter f_ε was varied, with f_k kept fixed as 0.2. Their results indicated a decrease in range of scales with decreasing f_ε, due to the increased dissipation.

The current work evaluates the three aforementioned approaches for specifying f_ε ($f_\varepsilon = 1.0$, $f_\varepsilon = a \cdot f_k$ with $a = 2$ and $f_\varepsilon = f_k$) by applying them to a turbulent channel flow at both 'low' ($Re_\tau = 180$) and 'moderate' ($Re_\tau = 395$) Reynolds numbers. The results are compared to Direct Numerical Simulation (DNS) reference data by Moser et al. [6]. The results of the high Reynolds number approach were previously presented, together with LES results, in Klapwijk et al. [7]. Those results exhibited two clear regimes, based on the value of f_k. If the filter length described by f_k is smaller than the driving mechanism of the turbulent flow, proper results are obtained; if f_k is larger turbulent fluctuations are not resolved and a laminar result is obtained. In the current work only the values of f_k yielding a turbulent flow are considered, which are $f_k = 0.15$, 0.10 and 0.05. To maintain a distinction between modelling and numerical error, a strong aspect of PANS, f_k and f_ε are kept constant in time and space.

This paper consists of a description of the PANS model, an investigation of the theoretical effects of the approaches for specifying f_ε, after which the test case and the corresponding results are described.

2 PANS MODEL

2.1 Model formulation

The Partially-Averaged Navier-Stokes equations are obtained by filtering the continuity and momentum equations, thereby decomposing all instantaneous quantities, Φ, into a resolved, $\langle\Phi\rangle$, and a modelled (unresolved) component, ϕ, according to $\Phi = \langle\Phi\rangle + \phi$ [8]. The PANS equations for incompressible, single-phase flow are

$$\frac{\partial \langle u_i \rangle}{\partial t} = 0, \tag{1}$$

$$\frac{\mathrm{D}\langle u_i \rangle}{\mathrm{D}t} = \frac{\partial}{\partial x_j}\left[\nu\left(\frac{\partial \langle u_i \rangle}{\partial x_j} + \frac{\partial \langle u_j \rangle}{\partial x_i}\right)\right] + \frac{1}{\rho}\frac{\partial \tau(u_i,u_j)}{\partial x_j} - \frac{1}{\rho}\frac{\partial \langle p \rangle}{\partial x_i}. \tag{2}$$

In these equations u_i indicates the velocity components, p the pressure, ν the kinematic viscosity, ρ the density and $\tau(u_i,u_j)$ the sub-filter stress tensor which is modelled using Boussinesq's hypothesis,

$$\frac{\tau(u_i,u_j)}{\rho} = 2\nu_t\langle S_{ij}\rangle - \frac{2}{3}k\delta_{ij} \tag{3}$$

with ν_t the turbulence viscosity, $\langle S_{ij} \rangle$ the resolved strain-rate tensor, k the modelled turbulence kinetic energy, and δ_{ij} indicates the Kronecker delta. To close the set of equations a Reynolds Averaged Navier-Stokes (RANS) model is used. The PANS model in this work is based on the $k-\omega$ Shear-Stress Transport (SST) model [1, 9]. The transport equations of the SST model are reformulated including the modelled-to-total ratio of turbulence kinetic energy and dissipation rate

$$f_k = \frac{k}{K} \qquad \text{and} \qquad f_\omega = \frac{\omega}{\Omega} = \frac{f_\varepsilon}{f_k}. \tag{4}$$

This leads to the reformulated equations

$$\frac{\mathrm{D}k}{\mathrm{D}t} = P_k - \beta^* \omega k + \frac{\partial}{\partial x_j}\left[\left(\nu + \nu_t \sigma_k \frac{f_\omega}{f_k}\right)\frac{\partial k}{\partial x_j}\right], \tag{5}$$

$$\frac{\mathrm{D}\omega}{\mathrm{D}t} = \frac{\alpha}{\nu_t} P_k - \left(P' - \frac{P'}{f_\omega} + \frac{\beta\omega}{f_\omega}\right)\omega + \frac{\partial}{\partial x_j}\left[\left(\nu + \nu_t \sigma_\omega \frac{f_\omega}{f_k}\right)\frac{\partial \omega}{\partial x_j}\right] + 2\frac{\sigma_{\omega 2}}{\omega}\frac{f_\omega}{f_k}(1-F_1)\frac{\partial k}{\partial x_j}\frac{\partial \omega}{\partial x_j}, \tag{6}$$

with

$$P' = \frac{\alpha\beta^* k}{\nu_t} \qquad \text{and} \qquad \nu_t = \frac{a_1 k}{\max\left(a_1\omega; \langle S \rangle F_2\right)}. \tag{7}$$

For the model constants and auxiliary functions, F_1 and F_2, see Menter et al. [9], while for more details on the implementation of the PANS model used here, the reader is referred to Pereira et al. [5].

Note that the separation into a resolved and a modelled component is very similar to the LES approach. Both approaches can be classified as variable-resolution turbulence simulations but based on a different closure paradigm; the closure of PANS is viscosity-based (sub-filter viscosity is a function of the modelled flow field (k, ω)), whereas in LES the closure is grid-based (sub-filter viscosity is a function of the cut-off length scale (Δ)) [10]. Consequently, in contrast to LES, the cut-off length scale of the resolved flow is not predetermined in PANS. The physical resolution is only determined by the settings, this leads to an overlap between the PANS resolved and modelled spectra [10], as shown in Figure 1. Since the grid remains fixed, computations with an f_k larger than what the grid allows are comparable to an explicitly filtered LES although based on a different modelling framework. Computations with a very low f_k value are effectively an Implicit LES (under-resolved DNS).

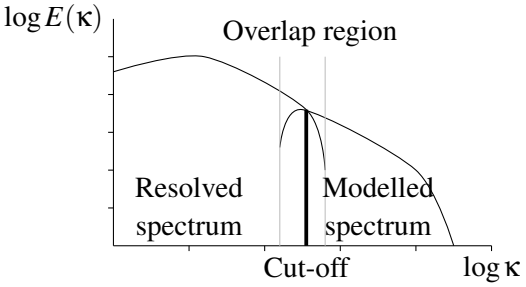

Figure 1: Schematic PANS wave-number energy spectrum, showing the overlap between resolved and modelled velocity scales. Based on Reyes et al. [10].

2.2 Specifying f_ε

Kinetic energy is mostly contained in the larger scales, whereas dissipation occurs in the smallest scales; this dictates $0 \leq f_k \leq f_\varepsilon \leq 1$ [4]. For specifying f_ε, three Reynolds number regimes can be distinguished in literature, which lead to different corresponding values of f_ε: the 'high', 'moderate' and 'low' Reynolds number approaches. Generally speaking in the high Reynolds number case, there is a clear separation between the large energy-containing scales and the small dissipative scales (identifiable by the inertial subrange, which follows Kolmogorov's law) [1, 3]. For a low Reynolds number flow these scales overlap. A moderate Reynolds number lies between these limits. In terms of scale separation, clearly this distinction is difficult to quantify. In generalised form, if f_ε is taken as $f_\varepsilon = a \cdot f_k$, the transport equations (5 and 6) reduce to

$$\underbrace{\frac{\mathrm{D}k}{\mathrm{D}t}}_{\mathrm{I}} = \underbrace{P_k}_{\mathrm{II}} \underbrace{-\beta^* \omega k}_{\mathrm{III}} + \underbrace{\frac{\partial}{\partial x_j}\left[\left(\nu + \nu_t \sigma_k \frac{a}{f_k}\right)\frac{\partial k}{\partial x_j}\right]}_{\mathrm{IV}}, \tag{8}$$

$$\underbrace{\frac{\mathrm{D}\omega}{\mathrm{D}t}}_{\mathrm{V}} = \underbrace{\frac{\alpha}{\nu_t} P_k}_{\mathrm{VI}} \underbrace{- \left(\left(1 - \frac{1}{a}\right) P' + \frac{\beta\omega}{a}\right)\omega}_{\mathrm{VII}} + \underbrace{\frac{\partial}{\partial x_j}\left[\left(\nu + \nu_t \sigma_\omega \frac{a}{f_k}\right)\frac{\partial \omega}{\partial x_j}\right]}_{\mathrm{VIII}} + \underbrace{2\frac{\sigma_{\omega 2}}{\omega}\frac{a}{f_k}(1 - F_1)\frac{\partial k}{\partial x_j}\frac{\partial \omega}{\partial x_j}}_{\mathrm{IX}}. \tag{9}$$

In the k equation (8), term (I) indicates rate of change plus convection, (II) rate of production, (III) rate of destruction and (IV) transport by molecular and turbulent diffusion. In the ω equation (9) the terms are rate of change (V), rate of production (VI), rate of destruction (VII), transport by molecular and turbulent diffusion (VIII) and cross-diffusion (IX). This last term is a result of the $\varepsilon = k\omega$ transformation in the construction of the SST model [11]. The terms in red differ from the standard SST model. For these equations the effect of the three approaches for specifying f_ε will be discussed from a numerical perspective. It is clear that terms (I), (II), (III), (V) and (VI) are independent of f_k and a.

High Reynolds number approach In this case $f_\varepsilon = 1.0$ ($a = 1/f_k$); here the transport by diffusion (IV and VIII) and cross-diffusion term (IX) increase proportionally to $1/f_k^2$ with decreasing f_k. The rate of destruction (VII) decreases proportionally to f_k. So for $f_k < 1.0$ the diffusion term in the k equation increases, spreading the modelled turbulent kinetic energy in space. At the same time, in the ω equation, the diffusion terms dominate over the destruction term. This implies that for low f_k values the dissipation is more spread out in space but the rate of destruction of ω is reduced.

Moderate Reynolds number approach In this case $f_\varepsilon = a \cdot f_k$ with $1.0 < a < 1/f_k$. Consequently terms (IV), (VIII) and (IX) increase proportionally to a/f_k. Term (VII) is independent of f_k and is proportional to a. Again the diffusion terms increase, and the destruction term in the ω equation decreases. The difference between these terms is smaller than for the high Reynolds number approach, so it is expected that dissipation occurs more locally.

Low Reynolds number approach In the limit of $f_\varepsilon = f_k$ ($a = 1.0$) terms (IV), (VIII) and (IX) increase proportionally to $1/f_k$. Term (VII) is now constant and reduces to $\beta\omega^2$, which is identical to the original SST model. The term containing P' disappears completely. With decreasing f_k the model remains identical to the SST model but with increased diffusion and cross-diffusion terms (IV, VIII and IX) [5].

Reyes et al. [10] derived the relationship between PANS and RANS turbulence viscosity as

$$\frac{\nu_{t,PANS}}{\nu_{t,RANS}} = \frac{f_k^2}{f_\varepsilon} \tag{10}$$

and related the PANS Kolmogorov scales to the physical integral scales for length (η/L), time (t_η/T) and velocity (u_η/U) as

$$\frac{\eta}{L} \sim C_\mu^{3/4} \frac{f_k^{3/2}}{f_\varepsilon}, \qquad \frac{t_\eta}{T} \sim C_\mu^{1/2} \frac{f_k}{f_\varepsilon}, \qquad \frac{u_\eta}{U} \sim C_\mu^{1/2} f_k^{1/2}. \tag{11}$$

The effect of the different approaches on these ratios across the f_k range is shown graphically in Figure 2, with $a = 2$ used throughout as example. Note that these ratios are independent of Reynolds number. The figure is corrected for the fact that f_ε cannot be not higher than f_k. The point after which the viscosity and length scales for $f_\varepsilon = 1.0$ and $f_\varepsilon = a \cdot f_k$ deviate, and where a discontinuity for the time scale is located, lies at $f_k = \frac{1}{a}$. For the turbulence viscosity and the length scales, the high Reynolds number approach yields the lowest ratios across the entire f_k range, meaning that the turbulence viscosity is lowered, more unsteadiness and smaller length scales can be expected in the solution. The moderate Reynolds number approach yields the same if $f_k > \frac{1}{a}$; for $f_k < \frac{1}{a}$ the turbulent viscosity and length scales are larger, i.e. it is expected that the smallest structures are absent. The low Reynolds number approach yields the highest ratio for all f_k except at the limits of $f_k = 0$ or 1. The time scales however show the opposite trend, across the f_k range the lowest ratio is for the moderate Reynolds approach. The low Reynolds number approach is independent of f_k, while the high approach lies in between these limits. The velocity scales decrease with $f_k^{1/2}$ independently of f_ε.

Note that for the high Reynolds number approach there is little difference in terms of turbulence viscosity and length scales if f_k is small (in the range $f_k < 0.2$). This corresponds to the findings in Klapwijk et al. [7], where only a fully developed turbulent solution was found for small f_k, but then little difference was seen between the different f_k values. In contrast, in this range the time scales are strongly affected.

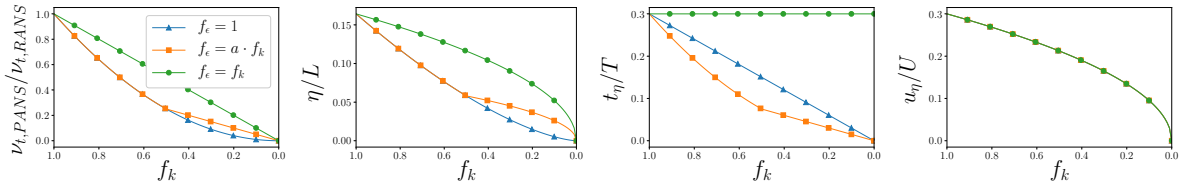

Figure 2: Relationship between PANS and RANS turbulence viscosity, ν_t, length, η_u/L, time, t_{η_u}/T, and velocity scales, u_{η_u}/U, versus f_k for different f_ε approaches. Here $a = 2$.

Based on these theoretical observations some questions arise concerning the use of the low Reynolds number approach. There appears to be no clear advantage; additional diffusion is added in the equations, and theoretically the the turbulent viscosity and length scales are larger than for the high Reynolds number approach, indicating that the smallest scales will be suppressed. For the moderate Reynolds number approach, small differences compared to $f_\varepsilon = 1.0$ are expected, and only for low f_k. In order to check these findings in a practical case, in the remainder of the paper the three approaches are applied to a turbulent channel flow at two different Reynolds numbers ($Re_\tau = 395$ and 180).

3 NUMERICAL SETUP AND SOLVER

The numerical setup has already been reported in Klapwijk et al. [7]. Computations are made using a rectangular domain, with two no-slip walls oriented normal to the y-axis (see Figure 3). The remaining boundaries are connected using periodic boundary conditions in order to approximate an infinite channel. Comparisons between different model settings are performed on a Cartesian grid, with a density of $N_x = 127$, $N_y = 95$ and $N_z = 95$ with clustering towards the walls. For $Re_\tau = 395$ this results in $x^+ \approx 12$, $y^+ \approx 0.1$ and $z^+ \approx 10$. The non-dimensional time step $\Delta t^* = \frac{u_\tau \Delta t}{2\delta} \approx 1 \times 10^{-3}$ leads to $\Delta t^+ = \frac{u_\tau^2 \Delta t}{\nu} \approx 0.08$ (2000 time steps per flow-through time). The grid density and time step are below LES guidelines and approach DNS resolution [12]. To maintain the proper bulk and friction Reynolds numbers, $Re_b = \frac{U_b 2\delta}{\nu}$ and $Re_\tau = \frac{u_\tau \delta}{\nu}$ respectively, a body force is applied which is proportional to the pressure gradient $\frac{\mathrm{d}p}{\mathrm{d}x} = -\frac{\tau_w}{\delta}$, with $\tau_w = \rho u_\tau^2$ [13]. The Péclet number has a magnitude of $O(10)$. As shown in the literature, the use of scale-resolving turbulence models for a turbulent channel yields a so-called supercritical laminar solution for which many flow-through times are needed to trigger transition to the turbulent regime [14]. In order to speed up the transition, the method suggested by Schoppa and Hussain [15] is used here. For more details, see Klapwijk et al. [7].

The numerical solver used for all simulations in this work is ReFRESCO, a multiphase unsteady incompressible viscous flow solver using RANS and Scale-Resolving Simulation models such as SAS, DDES/IDDES, XLES, PANS and LES approaches, complemented with cavitation models and volume-fraction transport equations for different phases (*www.refresco.org*). Time integration is performed implicitly using a second-order accurate scheme, all terms in the governing equations are discretised in space using second-order accurate central differencing, except for the convection terms of the turbulence equations, which use a first-order upwind scheme.

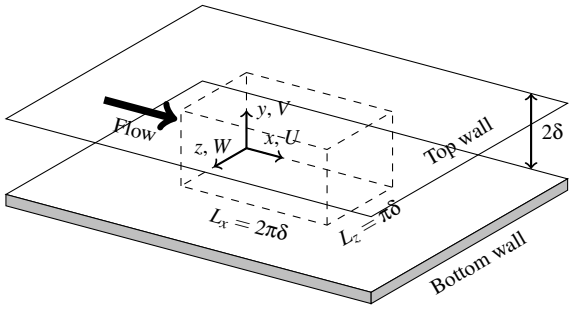

Symbol	Case 1	Case 2
Re_τ	395	180
Re_b	13800	6300
δ [m]	0.1	0.1
U_b [m/s]	6.928×10^{-2}	3.157×10^{-2}
u_τ [m/s]	3.966×10^{-3}	1.807×10^{-3}
τ_w [N/m^2]	1.570×10^{-2}	3.259×10^{-3}
ν [m^2/s]	1.004×10^{-6}	1.004×10^{-6}
ρ [kg/m^3]	998	998

Figure 3: Schematic overview of the domain and physical parameters. The dashed lines indicate the computational domain. The figure is based on the drawing of de Villiers [14].

4 NUMERICAL ERROR ESTIMATION

In order to verify the results the numerical errors were investigated. A distinction can be made between input, iterative, discretisation, and, in the case of unsteady computations, statistical errors. The input error is assumed to be negligible; the effect of the other error sources is investigated here.

Iterative error The residuals, normalised by the element on the diagonal of the matrix in the system of equations, were used to check the iterative convergence. Following the approach advocated by Eça et al. [16], a computation ($f_k = 0.10$, $f_\varepsilon = 1.0$) was performed using different iterative convergence criteria ($L_2 = 10^{-3}$, 10^{-4}, 10^{-5}, 10^{-6}, 10^{-7} and 10^{-8}). Five flow-through times are computed, starting

from a fully developed solution. Due to the limited number of flow-through times these results have a larger statistical error. The effect on the mean velocity ($\overline{u}/U_b$), Reynolds stresses ($Re_{ij} = \overline{u_i' u_j'}/u_\tau^2$) and turbulence kinetic energy spectra ($E_u(f)$ at $y^+ \approx 20$) is shown in Figure 4. The mean velocity appears almost unaffected; for the Reynolds stresses and spectra, $L_2 = 10^{-3}$ and 10^{-4} show a large mismatch with the reference data. The magnitude of the peak value Re_{uu} and the turbulence kinetic energy spectra converge for stricter convergence criteria towards the DNS data. As a compromise between cost and accuracy, the criterium $L_2 = 10^{-6}$ is used in the remainder of this work. This yields a negligible iterative error compared to the statistical error. Applying this criterium leads to a residual of $L_\infty = 10^{-5}$ in each time step for momentum. The residuals for pressure and turbulence equations are at least one order of magnitude smaller.

Discretisation error To assess the effect of the discretisation error, four different grids (with refinement ratios $r_i = h_i/h_1 = \Delta t_i/\Delta t_1 = 1.00$, 1.25, 1.57 and 1.97) were employed. The effect is again shown in Figure 4. Both the mean velocity and Reynolds stresses appear reasonably insensitive to grid resolution, only Re_{uu} deviates slightly on the finest grid. The main differences are observed for the turbulence kinetic energy spectra. Grid refinement leads to a slightly increased cut-off frequency, since the smaller cells allow for higher frequencies to be resolved. This indicates that the employed f_k (0.10) is below the grid cut-off, i.e. the grid is not at DNS resolution. Based on the similarity between the results it is concluded that the coarsest grid has a sufficient resolution.

Statistical error To remove the start-up effects and estimate the statistical uncertainty of the results, the Transient Scanning Technique is employed [17]. In Klapwijk et al. [7] it was concluded that the first 11 flow-through times must be removed to eliminate the start-up effects. The mean values are then computed based on approximately 45 flow-through times, resulting in a statistical uncertainty for the mean axial velocity between 0.5 and 2.5%, and for the Reynolds stress components between 5 and 10%. For more details the reader is referred to Klapwijk et al. [7].

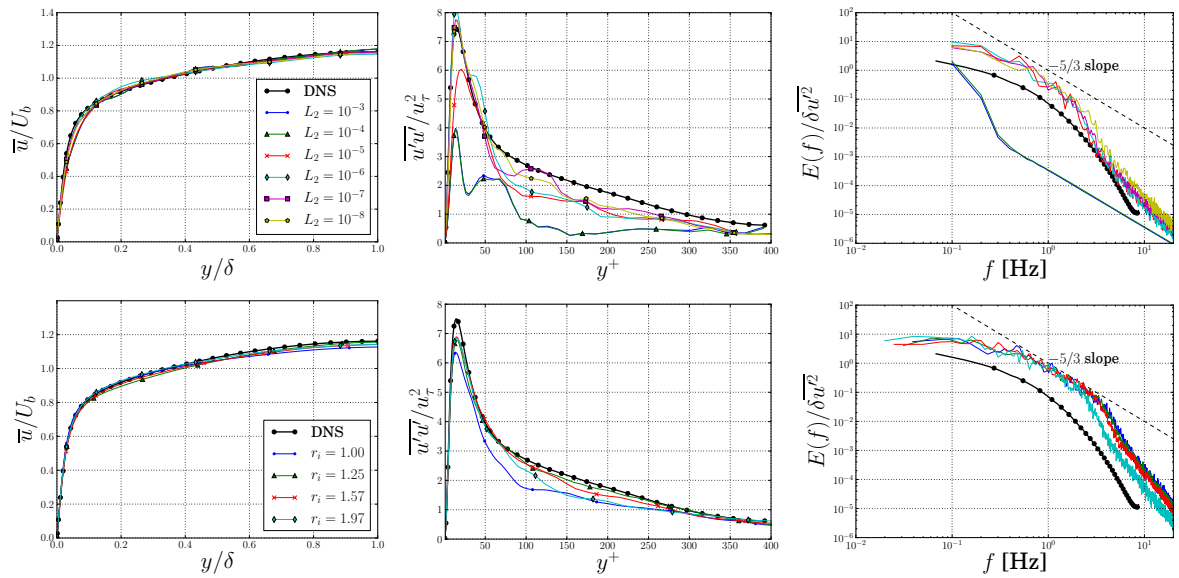

Figure 4: Mean velocity ($\overline{u}$) profiles, Reynolds stress (Re_{uu}) profiles and turbulence kinetic energy spectra ($E_{u,y^+\approx 20}(f)$) using different iterative convergence criteria (top row), and on different grids (bottom row).

5 RESULTS FOR DIFFERENT f_ε

For all figures in this section the three approaches ('high', 'moderate' and 'low' Reynolds number) are shown from left to right, indicated as H, M and L respectively. For M, f_ε is taken as $2 \cdot f_k$, i.e. $a = 2$. For $Re_\tau = 180$, the initialisation method (Section 3) yields a laminar flow for M and L. This is an indication of added dissipation (the initial perturbations are dampened). For comparison purposes, a second set of computations is performed where the computations are restarted from a fully turbulent H computation.

Figure 5 shows the mean velocity versus the channel height. For both Re_τ values H matches the DNS well independently of f_k. M shows slight discrepancies in the profile; especially for $Re_\tau = 180$, the velocity is underpredicted near the centre. L at $Re_\tau = 395$ and with $f_k = 0.15$ shows a more parabolic profile, which is an indication of a laminar flow. Both of the lower f_k values do show a turbulent flow profile, however the boundary layer appears to be thinner than half of the channel height. The velocity is almost constant in the region $0.5 \leq y/\delta \leq 1.0$. At the lower Re_τ, both $f_k = 0.15$ and 0.10 show a laminar profile. The profile for $f_k = 0.05$ matches the DNS data reasonably well.

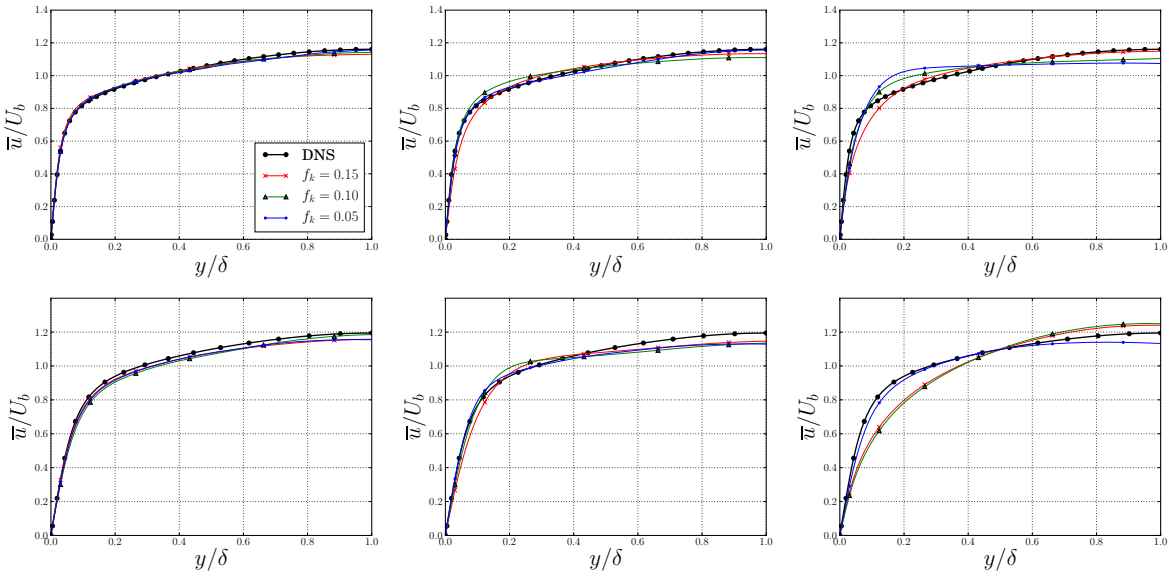

Figure 5: Velocity profiles ($\overline{u}/U_b$), from left to right H, M and L for $Re_\tau = 395$ (top) and 180 (bottom).

Figure 6 shows two components of the Reynolds stress profiles. The results for H and M are very similar. For both Re_τ, Re_{uu} and Re_{uv} both show the correct profile, the magnitude converges towards the DNS data with decreasing f_k. Re_{uv} is slightly underpredicted. Re_{uu} at $Re_\tau = 180$ is overpredicted near the wall for H and M. L clearly deviates from the reference data. At $Re_\tau = 395$, the Re_{uu} profiles show the correct shape, but $f_k = 0.15$ and 0.05 underpredict the magnitude. Re_{uv} is not captured by all f_k values. For $Re_\tau = 180$, the profile is correct for $f_k = 0.05$, although the magnitude is not well captured. For this Re_τ, $f_k = 0.05$ is again the only setting which captures Re_{uv} reasonably. For the other f_k settings, Re_{uv} is almost zero, indicating laminar flow, which is in agreement with the mean velocity profiles.

The turbulence kinetic energy spectra are shown in Figure 7. As expected the spectra at the lower Re_τ show less scale separation, while for the higher Re_τ, a $-5/3$ slope is observed in part of the frequency range. For H the value of f_k has little influence on the spectra, for M the effect of reducing f_k is more

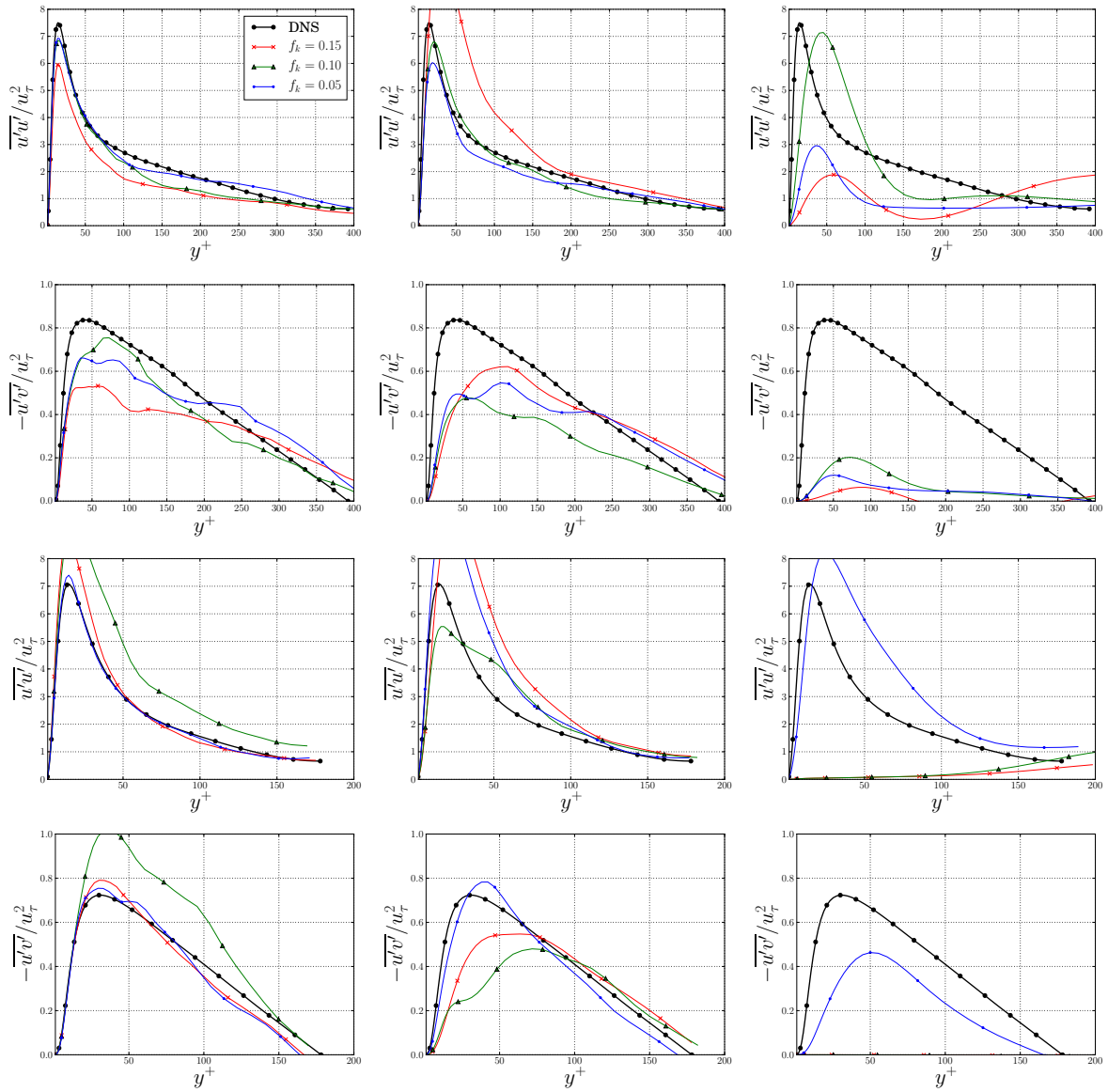

Figure 6: Normalised Reynolds stress profiles (Re_{ij}), from left to right H, M and L for $Re_\tau = 395$ (rows one and two) and $Re_\tau = 180$ (rows three and four).

visible. A lower f_k leads to more resolved turbulence, i.e. more energy in the spectrum and a higher cut-off frequency. This effect is the largest at $Re_\tau = 180$. The same influence of f_k is clear for L; only $f_k = 0.05$ at $Re_\tau = 180$ matches the reference set, but still the energy at higher frequencies is lower than for M and H. In all other computations the energy is too low, the spectrum shows again that the flow is mostly laminar. It is clear that reducing f_ε reduces the energy in the spectrum; M contains less energy than H, again especially at higher frequencies.

Finally the effect of f_ε on the flow is visualised using structures based on the Q-criterion in Figures 8 and 9 for $Re_\tau = 395$ and 180 respectively. For both Reynolds numbers the same observations are made;

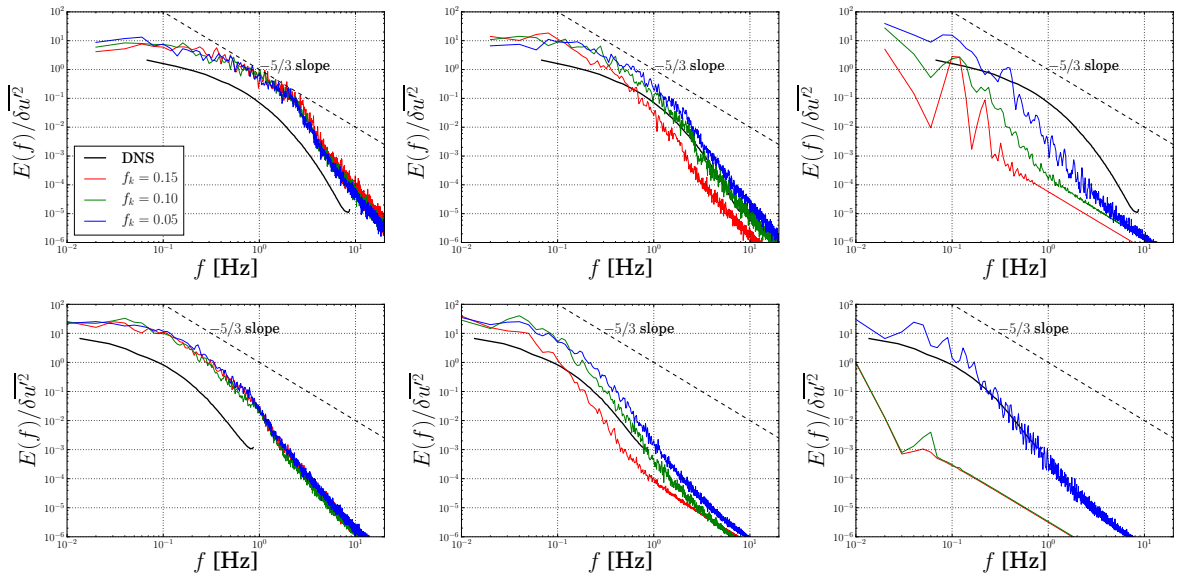

Figure 7: Turbulence kinetic energy spectra ($E_{u,y^+\approx 20}(f)$), from left to right H, M and L. $Re_\tau = 395$ (top row) and $Re_\tau = 180$ (bottom row).

for H the structures appear independent of f_k. M shows a large dependency on f_k; lowering f_k leads to more and smaller scales, for higher f_k only larger structures are observed away from the walls. This decrease in range of scales is in line with results by Frendi et al. [2]. The behaviour can be related to the definition of f_ε: for $f_\varepsilon = 1.0$, all dissipation occurs at the smallest scales, while if $f_\varepsilon < 1.0$, dissipation can also occur at larger scales. As a consequence the smaller scales are suppressed, since the turbulence is dissipated 'earlier'. By reducing f_k and thereby also f_ε the range of scales increases again. For L the absence of structures for $f_k = 0.15$ for both Re_τ, and for $f_k = 0.10$ for $Re_\tau = 180$ again indicates a laminar flow. $f_k = 0.10$ at $Re_\tau = 395$ shows some large structures, but these do not resemble the turbulent structures as seen for the other approaches or for LES simulations [7]. For $f_k = 0.05$ it is observed that the smallest structures are absent, which is in line with the turbulence kinetic spectrum.

6 CONCLUSIONS

Different approaches for specifying f_ε in the PANS model were compared based on theory and turbulent channel flow simulations. Little difference between the moderate and high Reynolds number approaches was found. The moderate Reynolds number approach does have a larger dependency on f_k, since due to the smaller value of f_ε, the turbulence dissipation is no longer confined to the smallest scales. For the low Reynolds number approach, it was demonstrated that excess diffusion is added to the equations. A laminar-like solution is obtained independent of the flow initialization or Reynolds number. It is concluded that even at a low Reynolds number, $f_k = f_\varepsilon$ is an approach which should not be used due to the suppression of the smaller scales. Only when using a very low f_k (in the DNS limit) reasonable results for the mean velocity and Reynolds stress profiles can be obtained, although in that case the results obtained using $f_\varepsilon = 1.0$ also match the reference data well for the present test case, and contain more energy at the smaller scales.

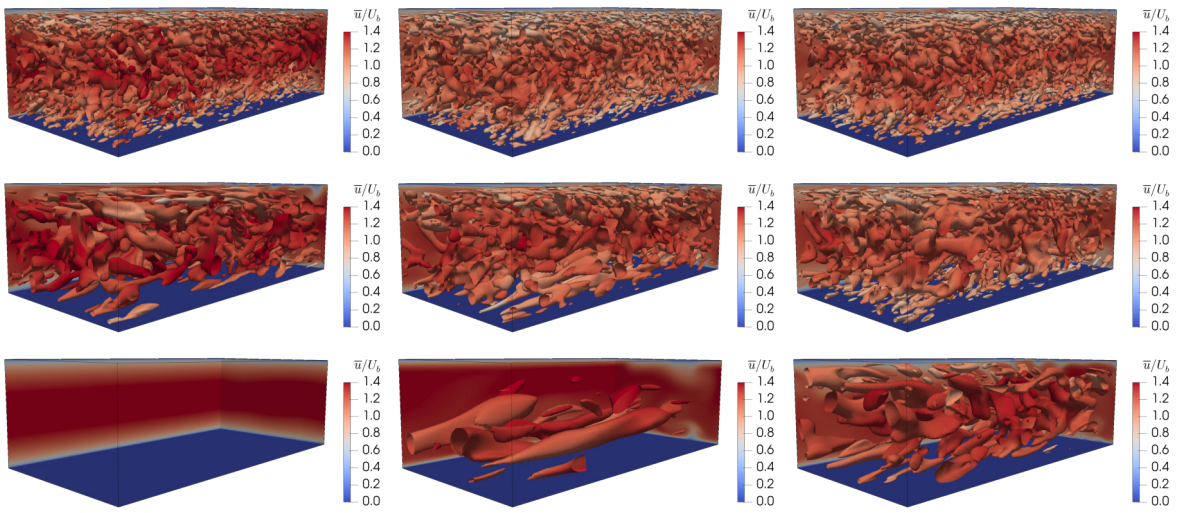

Figure 8: Instantaneous turbulent flow fields ($Q = 0.7$), coloured by $\overline{u}^* = \overline{u}/U_b$. From left to right $f_k = 0.15$, 0.10 and 0.05, for $f_\varepsilon = 1.0$ (first row), $f_\varepsilon = 2 \cdot f_k$ (second row) and $f_\varepsilon = f_k$ (third row). $Re_\tau = 395$.

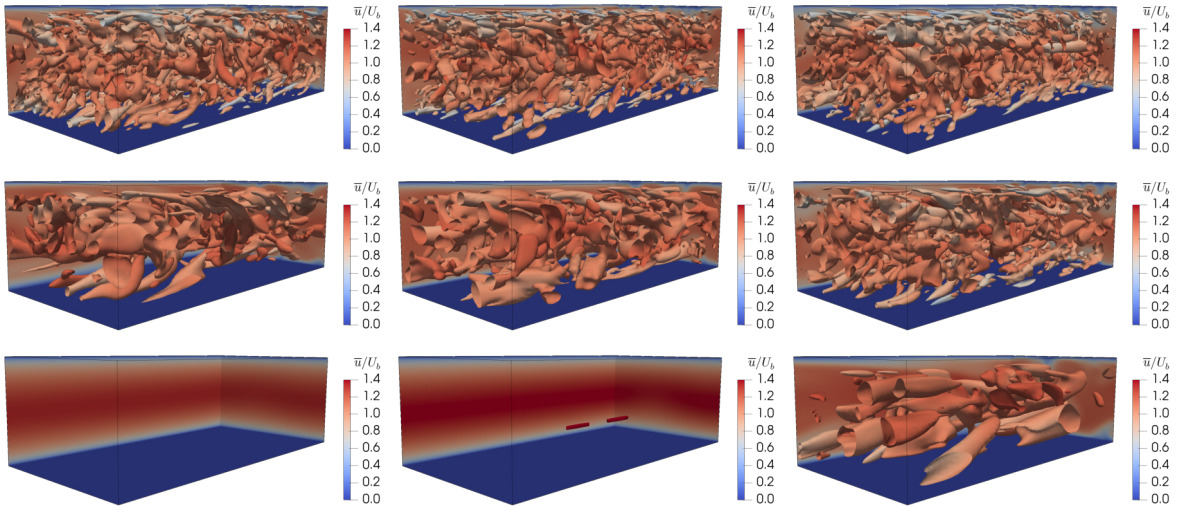

Figure 9: Instantaneous turbulent flow fields ($Q = 0.7$), coloured by $\overline{u}^* = \overline{u}/U_b$. From left to right $f_k = 0.15$, 0.10 and 0.05, for $f_\varepsilon = 1.0$ (first row), $f_\varepsilon = 2 \cdot f_k$ (second row) and $f_\varepsilon = f_k$ (third row). $Re_\tau = 180$.

For industrial flow cases at high Reynolds number, it is recommended to use $f_\varepsilon = 1.0$. That being said, if the reasoning is followed which leads to allowing f_k to vary in time and space, one can wonder whether the same should be applied to f_ε, i.e. f_ε depending on local flow quantities. There is currently no relationship to dynamically estimate f_ε found in the literature, while pursuing this method has the risk of re-introducing the problem of numerical and modelling error entanglement.

ACKNOWLEDGEMENTS

This research was financially supported by the Netherlands Organisation for Scientific Research, NWO, as part of the NOISOURCE project, and by the Dutch Ministry of Economic Affairs. The work was carried out on the Dutch national e-infrastructure, with the support of SURF Cooperative, on the *Reynolds* (TU Delft) and *Marclus3* (MARIN) clusters.

References

[1] F.S. Pereira, G. Vaz, L. Eça, and S.S. Girimaji. Simulation of the Flow Around a Circular Cylinder at Re=3900 with Partially-Averaged Navier-Stokes Equations. *International Journal of Heat and Fluid Flow*, 69, 2018.

[2] A. Frendi, A. Tosh, and S. Girimaji. Flow Past a Backward-Facing Step: Comparison of PANS, DES and URANS Results with Experiments. *International Journal for Computational Methods in Engineering Science and Mechanics*, 8(1):23–38, 2007.

[3] S. Lakshmipathy, D.A. Reyes, and S. Girimaji. Partially Averaged Navier-Stokes Method: Modeling and Simulation of Low Reynolds Number Effects in Flow Past a Circular Cylinder. In *6th AIAA Theoretical Fluid Mechanics Conference*, page 3107, 2011.

[4] S.S. Girimaji. Partially-Averaged Navier-Stokes Model for Turbulence: A Reynolds-Averaged Navier-Stokes to Direct Numerical Simulation Bridging Method. *Journal of Applied Mechanics*, 73(3):413–421, 2006.

[5] F.S. Pereira, G. Vaz, and L. Eça. An assessment of Scale-Resolving Simulation models for the flow around a circular cylinder. *Turbulence, Heat and Mass Transfer*, 8, 2015.

[6] R.D. Moser, J. Kim, and N.N. Mansour. Direct numerical simulation of turbulent channel flow up to $Re_\tau = 590$. *Physics of fluids*, 11(4):943–945, 1999.

[7] M. Klapwijk, T. Lloyd, G. Vaz, and T. van Terwisga. Channel Flow at $Re_\tau = 395$: LES is more (turbulent than PANS). In *21st Numerical Towing Tank Symposium (NuTTS'18), Cortona, Italy*, 2018.

[8] S.S. Girimaji and K.S. Abdol-Hamid. Partially averaged Navier-Stokes Model for Turbulence: Implementation and Validation. In *43rd AIAA Aerospace Sciences Meeting and Exhibit*, page 502, 2005.

[9] F.R. Menter, M. Kuntz, and R. Langtry. Ten years of industrial experience with the SST turbulence model. *Turbulence, heat and mass transfer*, 4(1):625–632, 2003.

[10] D.A. Reyes, J.M. Cooper, and S.S. Girimaji. Characterizing velocity fluctuations in partially resolved turbulence simulations. *Physics of Fluids*, 26(8):085106, 2014.

[11] H.K. Versteeg and W. Malalasekera. *An Introduction to Computational Fluid Dynamics The Finite Volume Method*. Pearson Education Limited, 2007. ISBN 9780131274983.

[12] N.J. Georgiadis, D.P. Rizzetta, and C. Fureby. Large-Eddy Simulation: Current Capabilities, Recommended Practices, and Future Research. *AIAA journal*, 48(8):1772–1784, 2010.

[13] S.B. Pope. *Turbulent Flows*. Cambridge University Press, 2000. ISBN 9780521598866.

[14] E. de Villiers. *The Potential of Large Eddy Simulation for the Modelling of Wall Bounded Flows*. PhD thesis, University of London, 2007.

[15] W. Schoppa and F. Hussain. Coherent structure dynamics in near-wall turbulence. *Fluid Dynamics Research*, 26(2): 119–139, 2000.

[16] L. Eça, G. Vaz, and M. Hoekstra. On the Role of Iterative Errors in Unsteady Flow Simulations. In *21st Numerical Towing Tank Symposium (NuTTS'18), Cortona, Italy*, 2018.

[17] J. Brouwer, J. Tukker, and M. Van Rijsbergen. Uncertainty analysis and stationarity test of finite length time series signals. In *The 4th International Conference on Advanced Model Measurement Technology for the Maritime Industry (AMT15), Istanbul, Turkey*, 2015.